[Chem. Pharm. Bull. 33(9)3935—3944(1985)]

Characteristics of Anion Transport Channels in the Human Erythrocyte. I. Interactions between Eosin 5-Isothiocyanate and Band 3 Proteins

YUKIO SATO,* TADAHIKO CHIBA, and YASUO SUZUKI

Pharmaceutical Institute, Tohoku University, Aobayama, Sendai 980, Japan

(Received December 20, 1984)

The interaction between eosin 5-isothiocyanate (EITC) and human erythrocyte ghosts has been studied by means of fluorescence and absorption difference spectroscopy. The fluorescence quenching data of the ghost–EITC system showed a biphasic change. EITC molecules bound to band 3 proteins and adsorbed on ghost membranes are responsible for this biphasic change. Binding of EITC molecules to the ghosts leads to a redshift and hypochromism in the visible region. Consequently, the difference spectrum shows a positive peak and two negative ones at 540, 517, and 483 nm from the longer wavelength side. The intensities of these peaks change heterogeneously under various conditions, reflecting the contributions of xanthene and phenyl chromophores bound to band 3. It was considered that the conformational structure of EITC binding sites is sensitive to temperature, showing a transition at about 30 °C. The reactivity of EITC molecules with band 3 at temperatures below 30 °C is different from that above 30 °C. It is inferred that the EITC binding sites on band 3 are identical with the modifier sites.

Keywords——human erythrocyte; ghost; anion transport; band 3; eosin 5-isothiocyanate; transport inhibitor; fluorescence quenching; difference spectrum

The anion transport system of the human erythrocyte membrane acts on permit bicarbonate formed from tissue CO_2 in the plasma.[1] In the lungs, the reverse reaction occurs in response to chloride exchange and the lowered CO_2 concentration. A 95000-dalton polypeptide, named band 3 on the basis of its relative mobility in sodium dodecyl sulfate gel electrophoresis, is responsible for the chloride exchange. Band 3 is a major integral protein of the erythrocyte and makes up about 25% of the total membrane proteins. This protein appears to exist in the membrane as a stable dimer.[2,3] Many studies have been made concerning the structure and function of band 3, and the mechanism of the anion-exchange catalyzed by band 3 has also attracted considerable attention.[4-10] Much evidence about the structure and mechanism of this system has been obtained by using stilbene-disulfonate derivatives which potentially inhibit the anion-exchange from the external side of the membrane. Several stilbene-disulfonates have been shown to react specifically with band 3 at a stoichiometry of one site per band 3 monomer.[11-16]

Cabantchik *et al.*[12b,c] presented a model that takes into account the available functional and structural evidence.[4,14] According to their model, the anion recognition site is composed of two positive charges and a hydrophobic area with electron-donor groups, and inhibitor compounds such as stilbene-disulfonates and phenyl-sulfonates bind *via* electrostatic and hydrophobic interactions and electron-donor–acceptor complexation. This is consistent with a polar site three-point-attachment configuration model.[17] It is considered that the cationic polar sites and nucleophilic groups located either in the hydrophobic pocket itself or adjacent to it are functional groups for anion transport. Beside this recognition site, the existence of an external "modifier" site was postulated.[18-20] Macara and Cantley[21] have presented a more mechanical model indicating that stilbene-disulfonates bind to a site on a band 3 monomer,

and they suggested that the modifier site may be part of a transport gate.

However, the relationship between the structure and function of the anion transport system has not yet been well established. Beside kinetic studies, characterization of the functional groups has not yet been investigated. We elected to investigate the properties of the functional groups by means of optical spectroscopic techniques. Here, we report the interaction between human erythrocyte ghosts and eosin 5-isothiocyanate, which is an inhibitor of sulfate exchange in intact erythrocytes.[22]

Experimental

Materials——Eosin 5-isothiocyanate (EITC) was prepared by bromination of fluorescein-isothiocyanate according to the procedure of Cherry *et al.*[23a] without modification. Fluorescein-isothiocyanate (100 mg) from Tokyo Kasei Kogyo Co., Ltd. was suspended in 2.0 ml of ethanol. Bromine (350 mg) was added drop by drop, the suspension being thoroughly stirred throughout. A clear solution was obtained on formation of the dibromo product, and as the reaction proceeded further, a precipitate of the insoluble tetrabromofluorescein-isothiocyanate was formed. After standing for 2 h at room temperature, the mixture was filtered and insoluble material was washed with 10 ml of ethanol. The product was solubilized in 10 mM phosphate buffer, pH 7.4, and precipitated at 4 °C with 1 N phosphoric acid. The precipitate was collected by centrifugation and washed three times with distilled water. After lyophilization, the product was stored at −20 °C until used. Its purity was confirmed by thin layer chromatography. *Anal.* Calcd for $C_{21}H_8Br_4NO_5S$: C, 35.78; H, 1.00; Br, 45.34; N, 1.99; S, 4.54. Found: C, 35.52; H, 1.03; Br, 45.45; N, 1.78; S, 4.59.

Preparation of Labeled Ghosts——Fresh human blood was obtained from Miyagi Prefectural Red Cross Blood Center. Red blood cells were washed three times with 310 ideal miliosmolarity (mosM) sodium phosphate buffer, pH 7.4. Packed cells (15 ml) were incubated with 3 mg of EITC for 3 h at 22 °C. The cells were then washed twice more with isotonic buffer to remove any unreacted label and subsequently hemolyzed in 40—50 volumes of 20 mosM sodium phosphate buffer, pH 7.4. The ghosts were sedimented by centrifugation for 20 min at 20000 *g* and washed three to four times with 20 mosM buffer. All operations except the labeling step were carried out at 0—4 °C.[23c] The optical properties of the samples prepared by this method were qualitatively consistent with those of the material prepared by the following method. In this study, therefore, the samples were obtained by the following procedure. Resealed erythrocyte ghosts were prepared by the standard method of Dodge *et al.*[24] Erythrocyte ghosts were incubated with various concentrations of EITC in the dark at 37 °C in 310 mosM phosphate buffer, pH 7.4. The solutions were subjected to spectral measurements at appropriate incubation times.

Liposomes——Unilamellar vesicles of phosphatidylcholine from egg yolk were prepared by the sonication method.

Spectral Measurements——The fluorescence and absorption spectra were taken on a JASCO FP-550 recording spectrofluorometer and a Hitachi 220 spectrophotometer, respectively. The measurements were carried out in quartz cells of 2, 5, or 10 mm path length at room temperature unless otherwise specified. The molar extinction coefficient, ε, was calculated on the basis of the initial concentration of EITC. The concentration of ghost membrane proteins was determined by the method of Lowry *et al.*[25] with bovine serum albumin as the standard. When the mean residue weight of 130 was used to compute the ellipticity at 223 nm of the membrane proteins, it was found that the ghost solution of 1×10^{-3} M (20 mosM phosphate buffer, pH 7.4) contained about 0.13 mg proteins per ml.[26] In this study, the concentration of the ghost solution is expressed in terms of mol/l. Each reported spectrum is the average of at least three separate protein samples, and the spectrum of each was recorded at least twice.

Results

Interaction of EITC with Ghost Membranes

Although EITC inhibits sulfate exchange in intact erythrocytes, EITC fails to produce more than about 80% inhibition in labeling for up to 3 h.[22] Nigg *et al.*[22] proposed that EITC may be less specific for band 3 at higher labeling strengths. In order to determine the extent of binding of EITC molecules to ghosts, the fluorescence spectra of ghost–EITC systems were measured. The binding of EITC to ghosts resulted in a decrease of fluorescence intensity (Fig. 1). This result is in contrast with that of ghost–stilbene disulfonate systems, in which a fluorescence enhancement upon binding to the inhibitory site on erythrocyte ghosts is observed.[21a,27] In Fig. 1, the fluorescence change of the liposome–EITC system is also shown. With increasing egg yolk phosphatidylcholine liposome concentration, the binding of EITC to

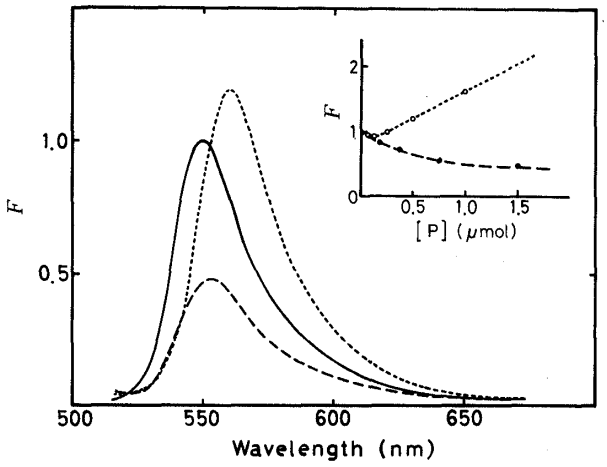

Fig. 1. Fluorescence Spectra of EITC in 310 mosM Phosphate Buffer (pH 7.4) at 25 °C

[EITC] = 1×10^{-5} M; [ghost] = 1×10^{-3} M (0.13 mg proteins/ml). (——), EITC alone; (— —), EITC in the presence of ghosts; (– – – –), EITC in the presence of egg yolk phosphatidylcholine liposomes.

Inset: The fluorescence change of EITC on binding to ghost membranes and liposomes. (—●—), in the presence of ghosts; (---○---), in the presence of liposomes.

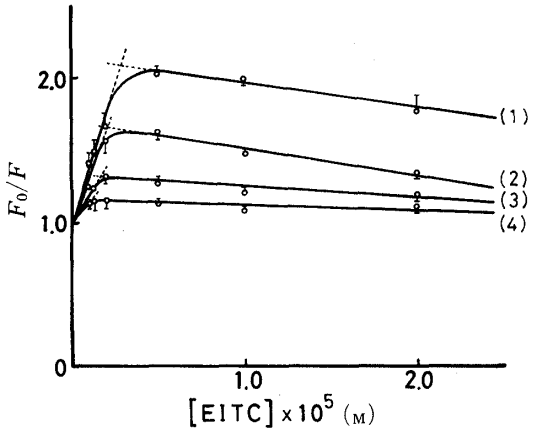

Fig. 2. Quenching of EITC Molecules by Binding to Ghosts of Various Concentrations

The data are means of three determinations. (1), [ghost] = 1×10^{-3} M (0.13 mg protein/ml); (2), [ghost] = 5×10^{-4} M; (3), [ghost] = 2.5×10^{-4} M; (4), [ghost] = 1.25×10^{-4} M.

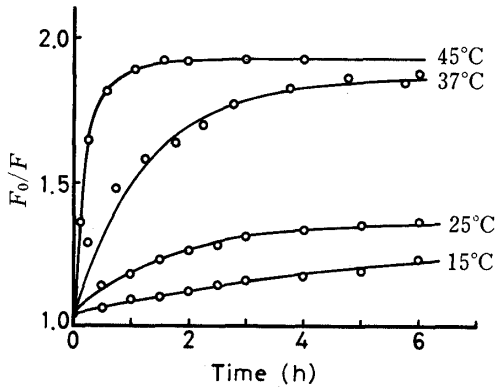

Fig. 3. Time Course of EITC Binding to Ghosts at Various Temperatures

The data were obtained from changes of EITC fluorescence intensity. The curves were calculated by means of the equation $y = a_1 + a_2(1 - e^{-kt})$.

[EITC] = 2×10^{-6} M; [ghost] = 1×10^{-3} M (0.13 mg proteins/ml). At 15 and 25 °C, values of $k = 0.14$ and $k = 0.6$ were assumed, ($a_1 = 1.04$, $a_2 = 0.32$). At 37 and 45 °C, values of $k = 0.8$ and $k = 2.9$ were assumed, respectively ($a_1 = 1.04$, $a_2 = 0.89$).

liposomes initially showed a decrease of intensity and then the intensity increased with a shift of the fluorescence maximum (Fig. 1 (inset)). In the liposome–EITC system, EITC molecules are adsorbed on the liposome membranes of low polarity. The decrease of intensity at lower concentration of liposomes might result from a local aggregation of EITC molecules on liposomes. On the other hand, the fluorescence quenching in the ghost–EITC system may be due to a transfer of electronic excitation energy from bound EITC to membrane proteins.

Figure 2 shows the Stern–Volmer plots for the quenching of EITC molecules in the ghost–EITC systems under various conditions. It is clear that the Stern–Volmer plots are biphasic. The position of the break is dependent on the ghost concentration. These results indicate the presence of more than one type of fluorophore. Cherry *et al.*[23b,c] proposed that EITC binds almost exclusively to band 3. Thus, it can be said that the biphasic Stern–Volmer plots are due to two types of binding environments for EITC molecules.

The time courses of EITC binding to ghosts are shown in Fig. 3. They correspond to the reaction curves of irreversible EITC binding to band 3. The curves can be expressed by the equation:

$$y=a_1+a_2(1-e^{-kt}) \quad (1)$$

where a_1 and a_2 represent constants, y is the ratio of fluorescence intensity at time t, and k is a rate constant. At $t=0$, $y=a_1$; at $t=\infty$, $y=a_1+a_2$. It appears that the curves can be classified into two groups according to temperature range, *i.e.*, higher than about 30 °C, and lower than 30 °C.

The absorption spectrum of EITC in phosphate buffer, pH 7.4, is shown in Fig. 4(a). The main band at 522 nm is due to local excitation of the xanthene ring.[28] Upon covalent binding to ghost proteins through the reactive isothiocyanate group, the absorption maximum shifted from 522 nm to the longer wavelength side, accompanied by a decrease in intensity. The change of the absorption spectrum results from the binding of EITC to band 3. Figure 4(b) shows a difference spectrum of the ghost–EITC solution. A positive peak and two negative peaks are observed at about 540, 517, and 483 nm. The changes of the three peaks in the difference spectrum can be used as an indicator of the reactivity of EITC with band 3.

Characteristics of the Difference Spectrum

The three peaks increased in intensity with the amount of ghosts (Fig. 5). Although the 540 nm peak increased without any shift, the 517 and 483 nm peaks shifted to higher energy. Such a binary change was not observed in the ghost–eosin Y system, in which no covalent binding occurs. The binary change is due to the different origins of the positive peak and the negative peaks. Such a difference of the spectral pattern may result from the presence of both reversible and irreversible binding. It seems that the changes of the 517 nm peak and 483 nm peak are parallel.

These results indicate that the behaviors of the positive and negative peaks reflect heterogenous interactions of the two chromophores with the binding sites in band 3. The positve and negative peaks may mainly reflect the interactions of the xanthene and phenyl rings with the functional groups in band 3, respectively. The xanthene chromophore should

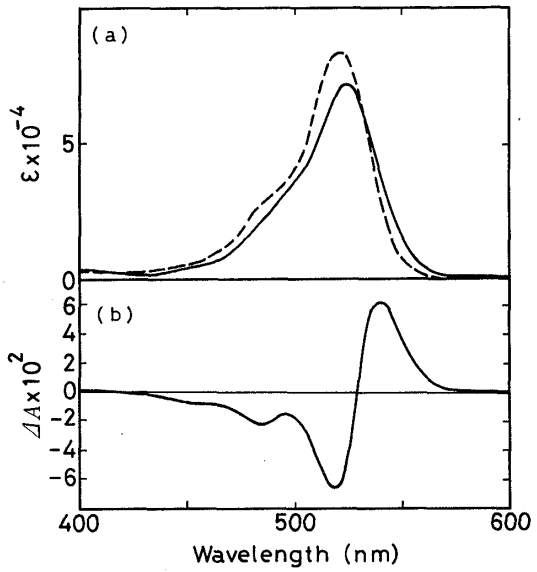

Fig. 4. (a) Absorption Spectra of the Ghost–EITC System and EITC in 310 mosM Phosphate Buffer (pH 7.4). (b) Difference Spectrum for Binding of EITC to Ghosts

[EITC] = 2×10^{-5} M; [ghost] = 1×10^{-3} M (0.13 mg proteins/ml). (——), ghost–EITC system; (----), EITC; cell length, 2 mm. The system was incubated for 5 h at 37 °C in the dark.

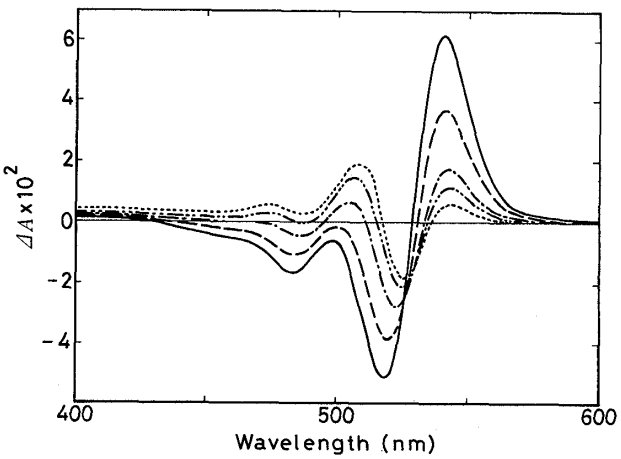

Fig. 5. Difference Spectra of the Ghost–EITC System at Various P/D Values

[EITC] = 2×10^{-5} M; cell length, 2 mm. (——), $P/D=50$; (— —), $P/D=25$; (—·—), $P/D=10$; (—··—), $P/D=5$; (----), $P/D=1$. The P/D indicates mol ratio of ghost protein to EITC.

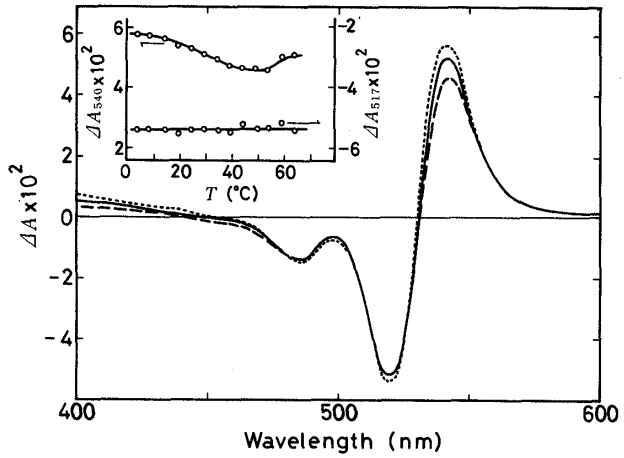

Fig. 6. Effects of Temperature on the Difference Spectra of Ghost–EITC System

[EITC] = 2×10^{-5} M; [ghost] = 1×10^{-3} M (0.13 mg proteins/ml); cell length, 2 mm. (----), at 4 °C; (——), at 25 °C; (— —), at 45 °C. The system was used after a 5 h incubation at 37 °C in the dark.

Inset: Plots of the intensities at 517 and 540 nm *vs.* temperature.

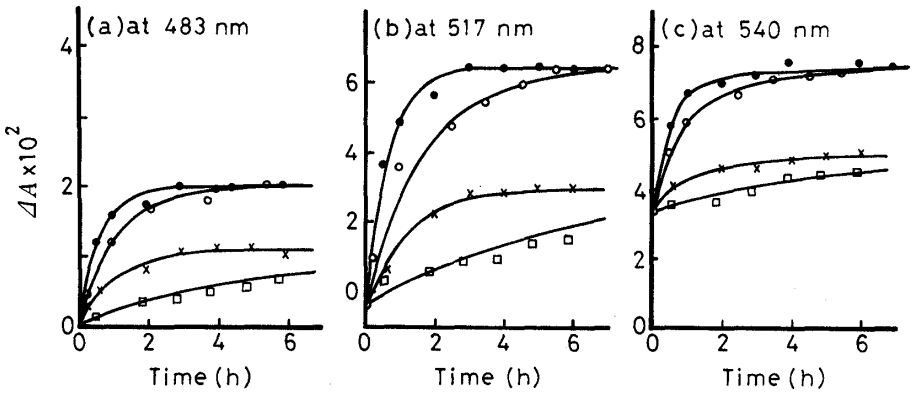

Fig. 7. Time Course of EITC Binding to Ghosts at Various Temperatures

[EITC] = 2×10^{-5} M; [ghost] = 1×10^{-3} M (0.13 mg proteins/ml); cell length, 2 mm. (—□—), at 15 °C; (—×—), at 25 °C; (—○—), at 37 °C; (—●—), at 45 °C. The data were obtained from intensity changes of difference spectra. The curves were calculated by means of the equation $y = a_1 + a_2(1 - e^{-kt})$. For the values of a_1, a_2, and k, see the text.

interact with the cationic polar site. On the other hand, the phenyl chromophore with the reactive isothiocyanate group should be covalently coupled to the nucleophilic centers.

The effects of temperature on these peaks were also examined for the ghost–EITC system incubated for 5 h at 37 °C in the dark. The results are shown in Fig. 6. Although the negative peaks were little affected by temperature, the positive peak was progressively increased with lowering of the temperature. A transition appears in the change of the positive peak at about 30 °C (Fig. 6 (inset)). Several explanations of this transition are possible. The first is that it is due to conformational change of the EITC-binding site. The second is that the transition is attributable to a thermal phase change of ghost membranes. The third is that the temperature effect is due to a change in band 3 mobility.[29] The 483 and 517 nm peaks behaved similarly. The differences in intensity changes may also reflect covalent binding of the phenyl chromophore to band 3 and the weak interaction of the xanthene chromophore.

Irreversible Binding of EITC

Figure 7 shows the reaction curves for the ghost–EITC system, obtained by treating the negative peaks as positive for convenience. The curves correspond to the time courses of irreversible EITC binding to band 3, as well as fluorescence intensity change (Fig. 3). Again, it is clear that the curves can be classified into two groups according to temperature range. As regards the curves for the 483 nm peak, at temperatures lower than 30 °C, the constants a_1 and a_2 are assumed to be 0 and 0.55, respectively, in Eq. 1. Then, the curves can be fitted by rate constant k values of 0.2 and 1.0 at 15 and 25 °C, respectively (Fig. 7a). At temperatures higher

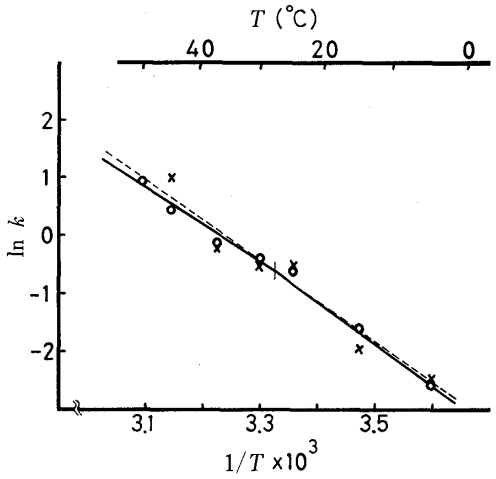

Fig. 8. Arrhenius Plots of the Rate Constants

(○), the means of k values obtained from the 483 and 540 nm peak changes; (×), k values obtained from the fluorescence change. The biphasic linear form of two intersecting straight lines yields a break point (T_b) at 27.5 °C, and activation enthalpy values of 12.0 kcal/mol above T_b ($r^2=0.8666$, $n=9$) and 15.1 kcal/mol below T_b ($r^2=0.9643$, $n=8$). The continuous line fitted to the same data gives an activation enthalpy value of 13.7 kcal/mol ($r^2=0.9637$, $n=13$).

Table I. Apparent Thermodynamic Parameters for the Interaction of Human Erythrocyte Ghosts with EITC

	ΔH^* (kcal/mol)	ΔS^* (cal/mol·degree)	ΔF^* (kcal/mol)	
Nonlinear model	15	−10	18	Below the transition
	12	−20	18	Above the transition
Linear model	14	−14	18	

than 30 °C, it can be assumed that a_1 and a_2 are 0 and 1.05, respectively, and the k values are 1.0 and 1.6 at 37 and 45 °C, respectively. The curves for the 517 and 540 nm peaks can also be classified into two groups according to temperature range (Figs. 7b and 7c). At temperatures lower than 30 °C, the values of a_1 and a_2 for the 540 nm peak curves can be assumed to be 1.65 and 0.80, respectively. Then, the k values are 0.2 and 0.8 at 15 and 25 °C, respectively. At the higher temperatures, a_1 and a_2 are 1.65 and 2.1, and the k values are 0.9 and 1.5 at 37 and 45 °C, respectively. The non-zero intercepts on the ordinate in Figs. 7b and 7c represent an initial rapid binding of xanthene chromophore. The fraction of rapidly occupied sites can be estimated as $a_1/(a_1+a_2)$. Thus, at lower temperatures, about 67% of the available binding sites seem to be occupied during the initial step of interaction. On the other hand, at the higher temperatures, about 44% of the binding sites are occupied. Thus, the initial rapid binding is dependent on temperature. Thereafter, the binding continues exponentially with the rate constant k, also depending on temperature and being classifiable into two cases. There is no intercept for the curves for the 483 nm peak, indicating that the phenyl chromophores are fixed during the slow binding process. These results show that the time course of irreversible binding of EITC to band 3 is biphasic overall. Similar biphasic processes of inhibitor binding were reported for 4,4′-diisothiocyanostilbene-2,2′-disulfonate (DIDS) and α,β-dihydro-4,4′-diisothiocyanostilbene- 2,2′-disulfonate (H_2DIDS) by Lepke *et al.*[13] For EITC binding to band 3, however, the slow binding process can be classified into two cases according to temperature.

The two kinds of binding reaction may correspond to the transition at 30 °C. Thus, we prepared Arrhenius plots of the rate constants for the reaction (Fig. 8). The rate constants obtained based on the change of fluorescence intensity are also plotted in Fig. 8. It should be noted that the characteristic properties of EITC bound to band 3 are not affected by the molecules bound to ghost membranes, since the fluorescence data were obtained at very low concentration of EITC as compared with the absorption data.

It seems that the temperature dependence of EITC binding is not well described by a single continuous line, and the plot has an apparent biphasic nature. From the biphasic form, apparent thermodynamic parameters were calculated for the two temperature ranges (classical analysis of nonlinear model). These values are listed in Table I.

Discussion

Interaction Profile of the Ghost–EITC System

We examined the properties of the EITC binding site to characterize the interaction profile of the ghost–EITC system by measuring fluorescence and absorption difference spectra under various conditions. The results presented here cast some light on the nature of the interaction of EITC with the anion transport system. At physiological pH, EITC is a dianion and might be expected to interact with the anion transport system of the erythrocyte.[22,30] EITC is an aromatic amphiphilic probe with hydrophobic character and a conjugation system, and it has an electrophilic substituent. Cabantchik *et al.*[4,14a] discussed the character of the interaction between benzene-sulfonates or stilbene-disulfonates and anion recognition sites. The results may be summarized as follows. 1) The interaction between anionic probes and the transport system involves a structured electrostatic binding component. 2) Hydrophobic pockets adjacent to or integrated in the cationic multipolar inhibitory sites anchor anionic amphiphiles. 3) Withdrawing electrons from putative membrane nucleophiles leads to donor–acceptor complex formation or binding to membrane ligands by H-bonding. 4) The π–π interactions betwen the aromatic ring and neighboring hydrophobic groups stabilize the anchoring of probes *via* lipophilic moieties. In other words, the chemical architecture of the anion transport system is composed of two positively charged sites, nucleophilic sites, and hydrophobic areas.

The Cabantchik model should be applicable to the interactions of band 3 with EITC, as well as other anionic amphiphilic compounds such as anthranil derivatives.[31]

From Fig. 3, the fraction of rapidly occupied sites at the lower and at the higher temperature regions was estimated at 76% and 54%, respectively. Both of these values are larger than those estimated from the difference spectra. This may be due to the presence of excess EITC molecules in the case of absorption spectroscopy. However, as can be seen in Fig. 8, the reactivity of EITC with ghosts was almost independent of EITC concentration. EITC molecules preferentially bind to band 3, and therefore, the reaction of EITC with ghosts under the present conditions should reflect the characteristics of the band 3–EITC reaction.

Binding Site of EITC

The binary Arrhenius plots of rate constants for EITC binding imply that EITC molecules are bound to and occupy different sites from H_2DIDS binding sites. The data in Table I show that the value of ΔS^* estimated at the higher temperature region is smaller than that at the lower temperature region, indicating that in the former case the degree of freedom in the initial step is smaller than that in the latter case. The activation enthalpy of 15 kcal/mol at the lower temperature region is smaller than that of H_2DIDS binding to band 3, 23 kcal/mol.[13] This may suggest a difference between the characteristic interaction of stilbene-disulfonates with band 3 and that of EITC. At the higher temperature region, the fixation of EITC on the target site in the early step results in decreasing entropy and there is a change of free energy in the reaction similar to that at the lower region. This implies that in the early process, hydrophobic interaction plays an important role in the band 3–EITC complex formation. Thus, although the structure of EITC binding site may be similar to the recognition site of stilbene-disulfonates, the EITC site is not exactly the same as the site for stilbene-disulfonates. According to Rao *et al.*,[27] the binding site of stilbene-disulfonates is

characterized by a hydrophobic and rigid environment with nearby tryptophan residues. This site is located in a protein cleft which extends some distance into the membrane. Nigg *et al.*[22] reported that 100% inhibition of sulfate transport is produced by DIDS, whereas a maximum of about 80% inhibition can be achieved by EITC. They suggested that EITC becomes less specific for band 3 at higher labeling strength. It seems more likely, however, that different binding sites are involved for DIDS and EITC. Since a decrease of tryptophan fluorescence at around 335 nm was observed in this study, the binding site of EITC may be nearby tryptophan residues. This suggests that the EITC binding site is close to the stilbene-disulfonate binding sites. We suggest that the binding site of EITC is the same as the modifier site, which is considered to be part of the transport gate.

Apparent Biphasic Arrhenius Plot

We will next consider whether Arrhenius plot is better fitted by the nonlinear model than by the linear model. Arrhenius plots which appear to consist of two straight lines intersecting at a "break" or "characteristic" temperature are frequently observed in membrane matrices.[32-34] According to Silvius and McElhaney,[35] nonlinear Arrhenius plots arise from a variety of mechanisms. Such Arrhenius plots can be described better by continuous "*Eb* (exponentially breaking)" functions than by two intersecting straight lines. From Fig. 8, it seems that discontinuous lines and a single continuous line can be equally well fitted to the data points. The *Eb* function is progressively more poorly approximated by two straight lines as ΔH^* or the temperature range of the Arrhenius plot increases or as the experimental error decreases. The usual limits of temperature variation in most biological studies are from about 5 °C to 40 °C. In the present study, the plots obtained from the difference absorption spectra showed a relatively small variation. Thus, we used 6 points for describing the data in terms of the continuous *Eb* function. The *Eb* function can be classified into four models.[35]

The first model is class I, in which the temperature dependence of ΔH^* is due to a finite heat capacity of activation. However, class I can be discarded, because no significant change is observed in the differential heat capacity scan of proteins in human erythrocyte ghosts below about 45 °C.[36]

The second and third models are termed classes II and III. In class II, the overall reaction rate is affected by multiple reaction steps. In class III, the protein undergoes a thermotropic conformational change which alters the activation parameters of the reaction. The last model is called class IV, in which the lipid environment of the protein changes with temperature and influences the reaction rate. According to Lepke *et al.*,[13] the Arrhenius plot for H_2DIDS binding to band 3 is linear. This indicates that the thermal phase change of ghost membranes does not influence the reaction rate. Thus, class IV and also the second explanation for the transition at 30 °C observed in the present study on the ghost–EITC system can be

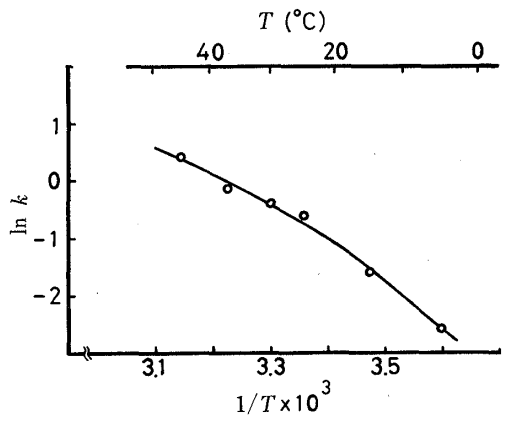

Fig. 9. Fitting the *Eb* Function to the Arrhenius Plot

The experimental data points in the Arrhenius plots shown in Fig. 8 ($5\,°C \leqq T \leqq 45\,°C$) were analyzed by means of the *Eb* function.

discarded.We will further consider the models based on classes II and III.

Figure 9 shows a theoretical Arrhenius plot corresponding to the *Eb* function derived for class III:

$$\ln k = -\Delta G^*/RT - \ln[1+\exp(\Delta H_c/R(1/T-1/T_0))] \quad (2)$$

where T is the absolute temperature and T_0 is the characteristic temperature. In this equation, it is assumed that the enthalpy of the conformational change ΔH_c is equal to the difference between the enthalpy changes in two conformations ($\Delta(\Delta H^*)=\Delta H_1^*-\Delta H_2^*$). The fit of this function gives an r^2 of 0.9919 ($n=6$). The calculated parameters of the *Eb* function are: $\Delta G^*=-1.0\pm0.5$ kcal/mol and $\Delta H_c=9.3\pm1.5$ kcal/mol, and the characteristic temperature, T_c, is 36.3 ± 13.5 °C. The rate expression for class II can be obtained by replacement of ΔH_c in Eq. 2 by $\Delta(\Delta H^*)$, where $\Delta(\Delta H^*)=\Delta H_2^*-\Delta H_1^*$ and the rate constants for the two steps are equal at $T_c=\Delta(\Delta H^*)/\Delta(\Delta S^*)$. In classes II and III, the thermodynamic parameters can be calculated as the differences between the parameters of the proteins in the lower and upper temperature conformations or in two alternate reaction pathways with different activation enthalpies. From the best-fit curve, the values of $\Delta(\Delta H^*)$, $\Delta(\Delta S^*)$ and ΔG^* were evaluated as 9.3 kcal/mol, 30.1 cal/mol·degree and -1 kcal/mol, respectively. These results indicate that the fit of the linear model of Arrhenius plot is poorer than that of the nonlinear model. In class II, the rate constants for the two steps are equal at T_c. In class III, T_c corresponds to the mid point temperature of the conformational change. The value of characteristic temperature obtained from the discontinuous straight lines, 27.5 °C, is different from that obtained from the *Eb* function, 36.3 °C, because of the large $\Delta(\Delta S^*)$ value. These discrepancies may arise from a small change in ΔH^* and from experimental error.

Nigg and Cherry[29] reported that rotational diffusion of band 3 depends on temperature, showing a biphasic decay of absorption anisotropy of eosin 5-maleimide or EITC labeled band 3 in erythrocyte membranes. They proposed that the biphasic change of mobility in the membranes may be due to a temperature-dependent self-aggregation of band 3. Such temperature-dependent association seems to be mediated either by a protein conformational change or by lipid phase segregation. On the other hand, it has been proposed that the modifier site should be sensitive to conformational change related to transport.[37] In view of these considerations, it seems most logical to conclude that the biphasic Arrhenius plot and the transition may be a result of a conformational change of the EITC binding site. This sensitivity should reflect the temperature dependence of EITC binding to band 3, supporting the inference of modifier site binding of EITC molecules. Such considerations seem to be consistent with the conformational changes which are related to the anion-transport function of band 3.[38] The characteristic break should reflect a limiting property of the EITC binding site.

References

1) J. O. Wieth, J. Brahm, and J. Funder, *Ann. N. Y. Acad. Sci.*, **341**, 394 (1980).
2) E. Nigg and R. J. Cherry, *Nature* (London), **277**, 493 (1979).
3) R. A. F. Reithmeier, *J. Biol. Chem.*, **254**, 3054 (1979).
4) Z. I. Cabantchik, P. A. Knauf, and A. Rothstein, *Biochim. Biophys. Acta*, **515**, 239 (1978).
5) *a*) H. Nakashima and S. Makino, *J. Biochem.* (Tokyo), **87**, 899 (1980); *b*) *Idem, ibid.*, **88**, 933 (1980).
6) A. Rothstein, M. Ramjeesingh, S. Grinstein, and P. A. Knauf, *Ann. N. Y. Acad. Sci.*, **341**, 433 (1980).
7) K. C. Appell and P. S. Low, *J. Biol. Chem.*, **256**, 11104 (1981).
8) S. Makino, H. Nakashima, and K. Shibagaki, *J. Biochem.* (Tokyo), **89**, 651 (1981).
9) S. Markowitz and V. T. Marchesi, *J. Biol. Chem.*, **256**, 6463 (1981).
10) H. Ideguchi, H. Matsuyama, and N. Hamasaki, *Eur. J. Biochem.*, **125**, 665 (1982).
11) A. H. Maddy, *Biochim. Biophys. Acta*, **88**, 390 (1964).
12) *a*) Z. I. Cabantchik and A. Rothstein, *J. Membrane Biol.*, **10**, 311 (1972); *b*) *Idem, ibid.*, **15**, 207 (1974); *c*) *Idem,*

ibid., **15**, 227 (1974).
13) S. Lepke, H. Fasold, M. Pring, and H. Passow, *J. Membrane Biol.*, **29**, 147 (1976).
14) *a*) M. Barzilay, S. Ship, and Z. I. Cabantchik, *Membr. Biochem.*, **2**, 227 (1979); *b*) M. Barzilay and Z. I. Cabantchik, *ibid.*, **2**, 255 (1979).
15) M. Ramjeesingh, A. Gaarn, and A. Rothstein, *Biochim. Biophys. Acta*, **641**, 173 (1980).
16) O. Fröhlich, *J. Membrane Biol.*, **65**, 111 (1982).
17) L. Aubert and R. Motais, *J. Physiol.* (London), **246**, 159 (1975).
18) M. Dalmark, *J. Gen. Physiol.*, **67**, 223 (1976).
19) *a*) P. A. Knauf, S. Ship, W. Breuer, L. McCulloch, and A. Rothstein, *J. Gen. Physiol.*, **72**, 607 (1978); *b*) P. A. Knauf, W. Breuer, L. McCulloch, and A. Rothstein, *ibid.*, **72**, 631 (1978).
20) R. B. Gunn and O. Fröhlich, *J. Gen. Physiol.*, **74**, 351 (1979).
21) *a*) I. G. Macara and L. C. Cantley, *Biochemistry*, **20**, 5095 (1981); *b*) *Idem, ibid.*, **20**, 5695 (1981).
22) E. Nigg, M. Kessler, and R. J. Cherry, *Biochim. Biophys. Acta*, **550**, 328 (1979).
23) *a*) R. J. Cherry, A. Cogoli, M. Oppliger, G. Schneider, and G. Semenza, *Biochemistry*, **15**, 3653 (1976); *b*) R. J. Cherry and G. Schneider, *ibid.*, **15**, 3657 (1976); *c*) R. J. Cherry, A. Burkli, M. Busslinger, G. Schneider, and G. R. Parish, *Nature* (London), **263**, 389 (1976).
24) J. T. Dodge, C. Mitchell, and D. J. Hanahan, *Arch. Biochem. Biophys.*, **100**, 119 (1963).
25) O. H. Lowry, N. J. Rosebrough, A. L. Farr, and R. J. Randall, *J. Biol. Chem.*, **193**, 265 (1951).
26) A. S. Gordon, D. F. H. Wallach, and J. H. Straus, *Biochim. Biophys. Acta*, **183**, 405 (1969).
27) A. Rao, P. Martin, R. A. F. Reithmeier, and L. C. Cantley, *Biochemistry*, **18**, 4505 (1979).
28) K. Hirano, *Bull. Chem. Soc. Jpn.*, **56**, 850 (1983).
29) E. A. Nigg and R. J. Cherry, *Biochemistry*, **18**, 3457 (1979).
30) F. Rypáček, J. Drobník, and J. Kálal, *Anal. Biochem.*, **104**, 141 (1980).
31) *a*) J.-L. Cousin and R. Motais, *Biochim. Biophys. Acta*, **687**, 147 (1982); *b*) *Idem, ibid.*, **687**, 156 (1982).
32) J. Brahm, *J. Gen. Physiol.*, **70**, 283 (1977).
33) J. R. Silvius and R. N. McElhaney, *Proc. Natl. Acad. Sci. U.S.A.*, **77**, 1255 (1980).
34) O. Eidelman and Z. I. Cabantchik, *J. Membrane Biol.*, **71**, 141 (1983).
35) J. R. Silvius and R. N. McElhaney, *J. Theor. Biol.*, **88**, 135 (1981).
36) S. R. Davio and P. S. Low, *Biochemistry*, **21**, 3585 (1982).
37) J. M. Salhany and P. B. Rauenbuehler, *J. Biol. Chem.*, **258**, 245 (1983).
38) H. Ginsburg, S. E. O'Connor, and C. M. Grisham, *Eur. J. Biochem.*, **114**, 533 (1981).